AGU PUBLICATIONS

JGR

Journal of Geophysical Research: Space Physics

RESEARCH ARTICLE
10.1002/2016JA022975

Key Points:
- A 1–10 eV ion loss from plasma wave interaction
- High-amplitude plasma waves seem like probable candidate
- Polarization analysis reveals that the waves are hiss

Correspondence to:
L. K. Sarno-Smith,
loisks@umich.edu

Citation:
Sarno-Smith, L. K., et al. (2016), Hiss or equatorial noise? Ambiguities in analyzing suprathermal ion plasma wave resonance, *J. Geophys. Res. Space Physics*, *121*, 9619–9631, doi:10.1002/2016JA022975.

Received 20 MAY 2016
Accepted 22 SEP 2016
Accepted article online 24 SEP 2016
Published online 13 OCT 2016

Hiss or equatorial noise? Ambiguities in analyzing suprathermal ion plasma wave resonance

Lois K. Sarno-Smith[1], Michael W. Liemohn[1], Ruth M. Skoug[2], Ondrej Santolik[3,4], Steven K. Morley[2], Aaron Breneman[5], Brian A. Larsen[2], Geoff Reeves[2], John R. Wygant[5], George Hospodarsky[6], Craig Kletzing[6], Mark B. Moldwin[1], Roxanne M. Katus[7], and Shasha Zou[1]

[1]Department of Climate and Space Sciences and Engineering, University of Michigan, Ann Arbor, Michigan, USA, [2]Los Alamos National Laboratory, Los Alamos, New Mexico, USA, [3]Department of Space Physics, Institute of Atmospheric Physics CAS, Prague, Czech Republic, [4]Faculty of Mathematics and Physics, Charles University in Prague, Prague, Czech Republic, [5]School of Physics and Astronomy, University of Minnesota, Twin Cities, Minneapolis, Minnesota, USA, [6]Department of Physics and Astronomy, University of Iowa, Iowa City, Iowa, USA, [7]Department of Mathematics, Eastern Michigan University, Ypsilanti, Michigan, USA

Abstract Previous studies have shown that low-energy ion heating occurs in the magnetosphere due to strong equatorial noise emission. Observations from the Van Allen Probes Helium Oxygen Proton Electron (HOPE) instrument recently determined that there was a depletion in the 1–10 eV ion population in the postmidnight sector of Earth during quiet times at $L < 3$. The diurnal variation of equatorially mirroring 1–10 eV H^+ ions at $2 < L < 3$ is connected with similar diurnal variation in the electric field component of plasma waves ranging between 150 and 600 Hz. Measurements from the Van Allen Probes Electric and Magnetic Field Instrument Suite and Integrated Science (EMFISIS) data set are used to analyze waves of this frequency in near-Earth space. However, when we examine the polarization of the waves in the 150 to 600 Hz range in the equatorial plane, the majority are right-hand polarized plasmaspheric hiss waves. The 1–10 eV H^+ equatorially mirroring population does not interact with right-hand waves, despite a strong statistical relationship suggesting that the two are linked. We present evidence supporting the relationship, both in our own work and the literature, but we ultimately conclude that the 1–10 eV H^+ heating is not related to the strong enhancement of 150 to 600 Hz waves.

1. Introduction

Thermal ions in the plasmasphere have been shown to be transversely heated through ion cyclotron resonance with waves above the ion gyrofrequency and below the lower hybrid resonant frequency. Ion cyclotron resonant heating of thermal ions was demonstrated through observations and modeling of GEOS 1 and GEOS 2 data [*Young et al.*, 1981; *Roux et al.*, 1982; *Perraut et al.*, 1982; *Perraut*, 1982]. In particular, He^+ was shown to most strongly resonate with the measured frequencies in the GEOS data. Other studies concluded that cyclotron resonance heats H^+ thermal populations at geosynchronous orbit similar to the He^+ heated population [*Quinn and Johnson*, 1982]. These thermal ions require left-hand or linearly polarized waves for wave-particle interactions that lead to subsequent heating. However, there is still a debate as to which waves are present during times of inner magnetosphere low-energy ion heating: equatorial noise or plasmaspheric hiss.

Equatorial noise has been shown to heat thermal ions through cyclotron resonance [*Olsen et al.*, 1987; *Singh and Hwang*, 1987; *Laakso et al.*, 1990]. Equatorial noise is a fast magnetosonic, low-frequency wave with nearly linearly polarized magnetic field fluctuations generated by unstable energetic proton ring velocity distributions [*Perraut et al.*, 1982; *Gary et al.*, 2010]. Equatorial noise ranges in frequency from approximately 20 Hz to a few hundred hertz and lies below the lower hybrid frequency [*Němec et al.*, 2015; *Boardsen et al.*, 2016]. Typically, equatorial noise is found between 2 and 7 Earth radii and within 10° of the magnetic equator [*Russell et al.*, 1970; *Němec et al.*, 2006]. Strong diurnal variation has been previously seen in Cluster observations of equatorial noise outside of the plasmasphere, with a peak at MLT = 12 and a minimum in the postmidnight sector between MLT = 0 and 6 [*Hrbáčková et al.*, 2015; *Ma et al.*, 2016]. Studies of the global wave distribution revealed that equatorial magnetosonic waves inside the plasmapause depended on

substorm activity and had larger amplitudes and higher occurrence frequencies on the dayside [*Green et al.*, 2005; *Meredith et al.*, 2008; *Ma et al.*, 2013].

Based on Dynamics Explorer 1 and SCATHA observations, it was proposed that equatorial noise, generated by highly energetic ions in the ring current and/or radiation belt, heats the thermal ion population through cyclotron resonance. Wave-particle interactions elevate the thermal population to a suprathermal population via energy deposition by equatorial noise (10 eV $< E <$ 300 eV) [*Curtis*, 1985]. The energy transference could also occur with 1–10 eV He^+ and O^+, albeit on slower timescales. Modeling work also suggests that inward propagating magnetosonic waves produced by proton ring instabilities could cause thermal plasma heating near Earth [*Horne et al.*, 2000].

However, plasmaspheric hiss occupies a similar region of space as the equatorial noise and typically ranges from 20 Hz to approximately 1000 Hz [*Thorne et al.*, 1973; *Meredith et al.*, 2007; *Li et al.*, 2015]. Plasmaspheric hiss is a broadband incoherent electromagnetic emission that is largely confined to Earth's plasmasphere [*Meredith et al.*, 2009]. Plasmaspheric hiss can be generated from magnetospherically reflecting whistler waves or from inward propagating chorus emissions that lose coherency when they cross the plasmapause [*Draganov et al.*, 1992; *Bortnik et al.*, 2008]. Hiss amplification at the equator due to wave turbulence from the electron gyroresonance instability leads to enhanced plasmaspheric hiss in the magnetic equatorial plane [*Thorne and Barfield*, 1976; *Church and Thorne*, 1983; *Solomon et al.*, 1988; *Santolik et al.*, 2001]. Unlike equatorial noise, plasmaspheric hiss is right-hand polarized and primarily interacts with electrons [*Tsurutani et al.*, 1975; *Li et al.*, 2007; *Summers et al.*, 2007]. Without looking at polarization or spectral lines, it is difficult to distinguish between plasmaspheric hiss and equatorial noise [*Gurnett*, 1976; *Santolík et al.*, 2002].

Plasma waves are a likely cause for the observed minimum in the high-energy tail (1–10 eV) of the inner plasmasphere (L shell < 3) in the postmidnight sector [*Lennartsson and Reasoner*, 1978; *Sarno-Smith et al.*, 2015]. A previous study revealed that in the postmidnight sector specifically, the H^+ pitch angle (PA) = 90° population between $2 < L < 3$ was depleted but plasma was still flowing upward from the ionosphere [*Sarno-Smith et al.*, 2016a]. Upward flowing plasma in the postmidnight sector suggests that the apparent loss of plasma in the postmidnight sector is not driven by the cooling of plasma in the topside ionosphere. Instead, plasma wave influence may be heating/scattering the particles in such a way to lead to strong diurnal variation in the 1–10 eV population.

Three instruments on board the NASA Van Allen Probes mission enable further exploration of the connection between 1–10 eV ions of the inner plasmasphere and plasma wave activity. The Van Allen Probes, launched in late 2012, are a pair of satellites that are in highly elliptical, low inclination orbits [*Mauk et al.*, 2014]. The Electric and Magnetic Field Instrument Suite and Integrated Science (EMFISIS) instrument measures plasma waves between approximately 2 Hz and 12 kHz using three search coil magnetometers and the three Electric Field and Waves (EFW) instrument's electric field antennas [*Wygant et al.*, 2013; *Kletzing et al.*, 2014]. EMFISIS also measures the DC magnetic field with onboard magnetometers. The plasma wave range we examine is between 150 Hz and 600 Hz, well within the resolution capabilities of EFW and EMFISIS. The Helium Oxygen Proton Electron (HOPE) instrument measures the ion and electron populations of the equatorial inner magnetosphere between 1 eV and 50 keV [*Funsten et al.*, 2014]. HOPE also uses the EMFISIS magnetometer measurements to map the observed fluxes into pitch angle space and assign nominal pitch angle bins.

We examine the connection between 150 Hz and 600 Hz waves with the 1–10 eV ion population of the $L < 3$ inner plasmasphere. As previous studies have found, we find that the diurnal variation in the 150–600 Hz waves is linked with the 1–10 eV ion equatorially mirroring population growth and loss [*Olsen et al.*, 1987; *Singh and Hwang*, 1987]. Polarization analysis reveals that the near-Earth emissions near the equator are primarily plasmaspheric hiss and do not cyclotron resonate with the low-energy ions and are not responsible for the ion heating. We corroborate our results with observations from EMFISIS and HOPE, opening up several questions in magnetospheric physics of our understanding of thermal plasma and wave interaction.

2. Particle and Wave Statistics

Following the 1–10 eV ion depletion in the postmidnight sector discovery in *Sarno-Smith et al.* [2015], we examine the fluxes measured at different pitch angles from February 2013 to April 2015. The polar angle resolution on the HOPE instrument is 18° full width. Pitch angle bins are 18° wide, except for 9° bins centered at

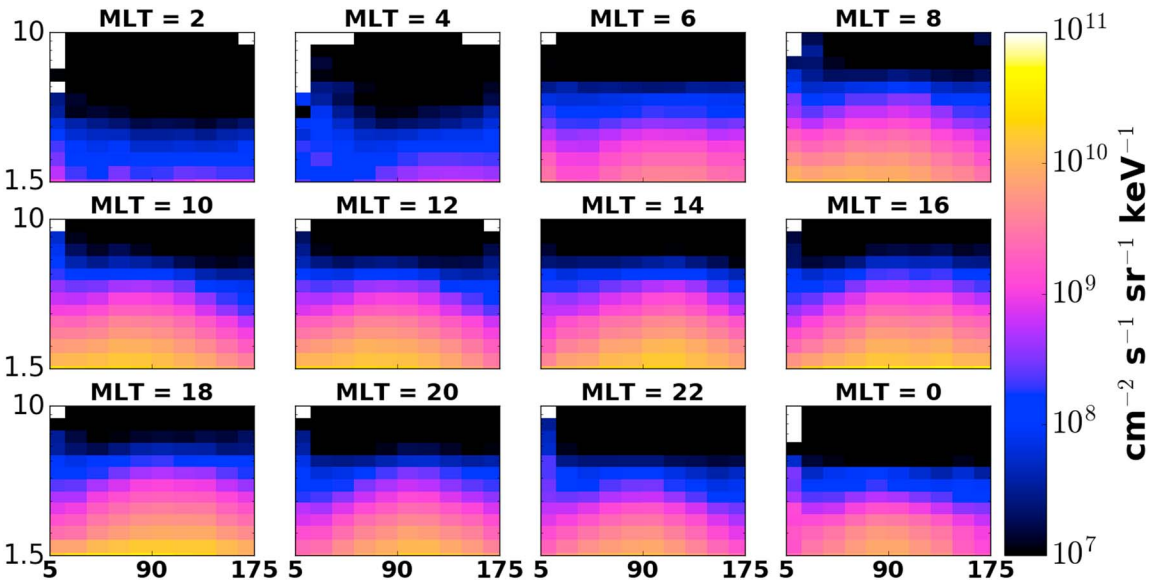

Figure 1. Median differential number fluxes corrected for spacecraft potential for 1.5–10 eV H^+ measured by HOPE at L = 2.5 at several MLTs from February 2013 to April 2015. The fluxes were binned by energy channel and pitch angle.

4.5 and 175.5°. In every spin period of approximately 11 s, HOPE differential number flux values were calculated and assigned a pitch angle designation based on the magnetic field direction as measured by EMFISIS. Initial analysis of the pitch angle distributions were conducted by *Sarno-Smith et al.* [2016b], and here the analysis is taken further to examine the evolution of the full velocity-space distribution in both energy and pitch angle.

Figure 1 displays the median 1–10 eV H^+ differential number fluxes at L = 2.5 for times when $Kp < 3$ between February 2013 and April 2015 measured by HOPE sorted by pitch angle, MLT, and energy. The fluxes are corrected for spacecraft charging, and the process is detailed in *Sarno-Smith et al.* [2016b]. We note that the Van Allen Probes tend to charge slightly positive. The L = 2.5 bin spans from 2.375 to 2.625 (0.25 L shell). The fluxes are not always centered near PA = 90° due to seasonal effects, such as increased upwelling ion fluxes from the summer hemisphere compared to the winter hemisphere. At MLT = 2, the near PA = 90° population is at a minimum for all energies shown. The flux measurements at near PA = 0° and near PA =180° are lower compared with other MLTs for these pitch angle bins but are larger than the near PA = 90° measurements. The equatorially mirroring population begins to refill for the 1 eV energy channels at MLT = 4, but the near PA = 90° population minimum is prevalent at the higher energies (energy > 2 eV). MLT = 6 demarcates the transition from a dominant refilling population at 0° and 180° to a more equatorially mirroring focused population. Above 6 eV, however, the near PA = 90° population is still at a relative minimum compared to the 0° and 180° pitch angle flux measurements or the distribution is isotropic.

A balance is struck between MLT = 8 and MLT = 18 where the near PA = 90° population is still at a relative minimum above 8 eV, but the near PA = 90° population remains in a steady state throughout the day. MLT = 22 fluxes reveal that the equatorially mirroring population has begun to recede. While the near PA = 90° population still dominates below 3 eV, the pitch angle distributions are either refilling (0°/180° dominated) or isotropic beyond 3 eV. MLT = 0 exhibits similar behavior, with the last of the near PA = 90° population at 1.5 eV narrowing.

In Figure 1, there are two indications that the loss of the equatorially mirroring population may not simply be a balance of ionospheric outflow and scattering. The first indicator is if the change in 1.5–10 eV plasma in the inner magnetosphere was from ionospheric diurnal variation and consequent transport to the plasmasphere, it would be expected that the higher-energy ions should appear first at L = 2.5 and scatter first since they move the fastest. Instead, we see that the lowest energies for PA = 90° rise the fastest and the higher energies above 8 eV either never have a near PA = 90° population maximum or take longer than the lower energies. For example, the 2 eV equatorially mirroring population is at a maximum by MLT = 6, but the 8 eV population is not at a maximum until MLT = 8.

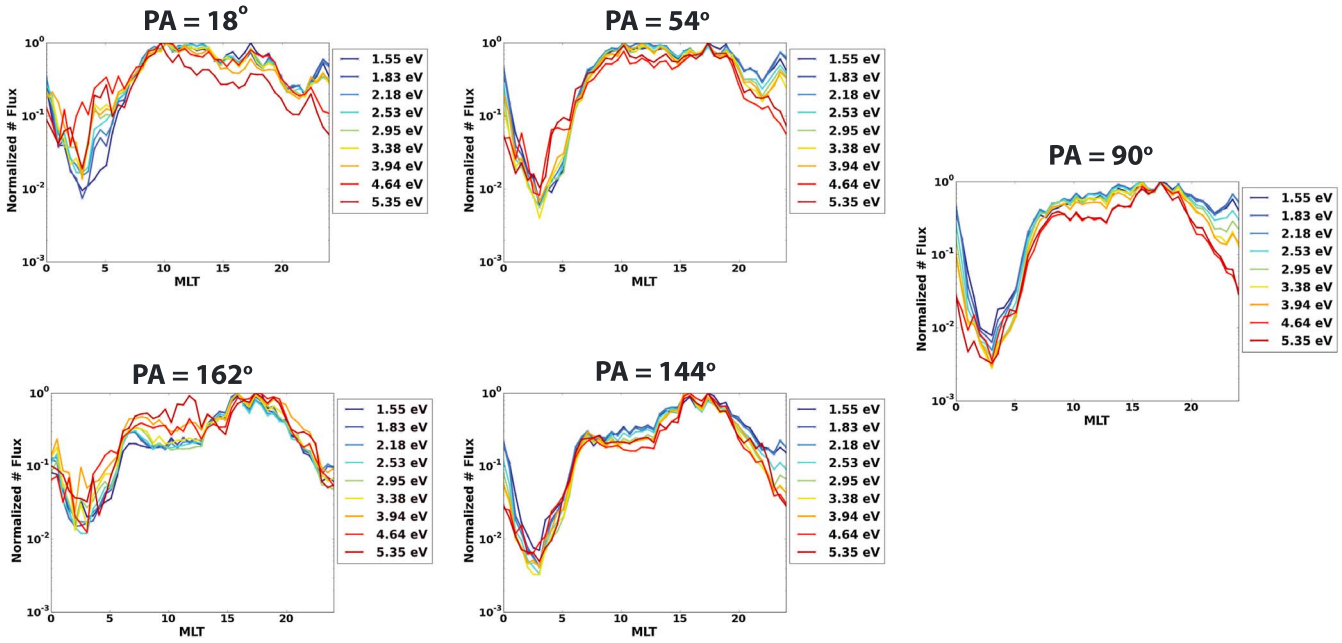

Figure 2. Normalized median differential number fluxes corrected for spacecraft potential for 1.5 eV, 1.83 eV, 2.18 eV, 2.53 eV, 2.95 eV, 3.38 eV, 3.94 eV, 4.64 eV, and 5.35 eV H^+ measured by HOPE at $L = 2.5$ from February 2013 to April 2015 for PA = 18°, 54°, 90°, 144°, and 162°. The median fluxes were normalized based on the maximum value for each energy at all MLTs.

The other indication is the depletion in the near PA = 90° population compared to the near PA = 0°/180° measurements. While the equatorially mirroring populations have >2.5 orders of magnitude of variation, the field-aligned fluxes show about 2 orders of magnitude diurnal variation. We use the 18° and 162° bins to describe the field-aligned PA bins because the 175.5° and 4.5° bins are smaller and less accurate. Figure 2 shows the $L = 2.5$ spacecraft potential corrected fluxes of 1.55, 1.83, 2.18, 2.53, 2.95, 3.38, 3.94, 4.64, and 5.35 eV normalized by the highest values at each energy at pitch angles of 18°, 54°, 90°, 144°, and 162°. For the more field-aligned pitch angles, the normalized fluxes show that the high-energy H^+ ions rise first at dawn compared to the slower particles. At PA = 90°, the opposite occurs, with the lowest energy fluxes increasing first.

The PA = 90° fluxes also show an energy-dependent decrease. Starting at MLT = 18, the PA = 90° fluxes start decreasing. The highest energy ions are depleted first, with over an order of magnitude drop occurring before midnight. The low-energy ions (1–3 eV) have a delayed depletion until the postmidnight sector. The steady growth of the PA = 90° population across the morning to a saturation point at MLT = 10 suggests perpendicular heating of the H^+ ions throughout the dayside. The flatness of the curves across the dayside at all pitch angles in Figure 2 indicates that the fluxes are in equilibrium, with the wave heating balanced by the scattering and loss.

From Figures 1 and 2, we can conclude that wave activity, not ionospheric breathing, is responsible for the 1–10 eV ion depletion because of the behavior of the PA = 90° population. Following the theory of equatorial noise heating thermal plasma from *Olsen et al.* [1987], we explore the possibility of a wave-particle interaction by examining the EMFISIS survey mode data over the course of 26 months. The survey mode on EMFISIS includes a set of spectral matrices every 6 s [*Kletzing et al.*, 2014]. The EMFISIS instrument uses a fast Fourier transform on board to analyze the electric field samples from EFW, and the results are telemetered to the ground. The EMFISIS survey mode data are averaged on board into 65 logarithmically spaced bins between 2 Hz and 10 kHz and binned by 0.5 MLT and 0.25 L shell for times when $Kp < 3$.

To identify peak wave activity, Figure 3 shows the relative intensity of EMFISIS WaveForm Receiver (WFR) frequencies as a function of MLT at $L = 2.5$. Figure 3a shows the median power spectral densities from February 2013 to April 2015. Figure 3b uses the same binning strategy and displays the normalized power spectral densities. The power spectral densities in each frequency bin are normalized by the highest power spectral density in that frequency bin. The silver line is the sixth harmonic of the H^+ cyclotron frequency. We use the

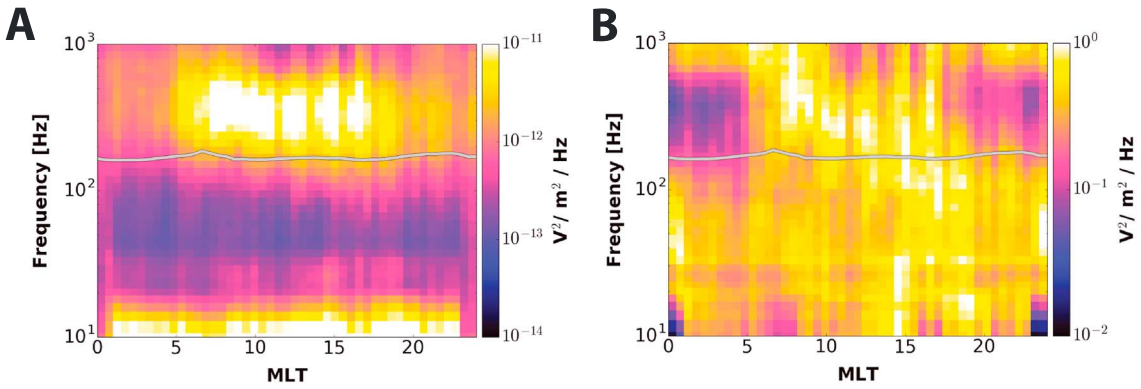

Figure 3. (a) The median power spectral density of the electric field component of waves measured from EMFISIS in 0.5 MLT bins and logarithmically spaced frequency bins between 10 Hz and 1 kHz from February 2013 to April 2015 at $L = 2.5$. (b) The power spectral density of the electric field wave component normalized across all MLTs by the maximum value at each frequency/0.5 MLT bin over the same time period at $L = 2.5$. In both Figures 3a and 3b, the silver line is the sixth harmonic of the H^+ cyclotron frequency.

sixth harmonic of the H^+ cyclotron frequency because it is approximately where we see enhanced power spectral densities. We show the geometric mean lower hybrid frequency instead of the lower hybrid frequency because it is difficult to get a true estimate on plasma density at $L < 3$, where EMFISIS electron number density estimates from the upper hybrid frequency saturate [*Kurth et al.*, 2015]. This technique has been used in previous studies to estimate the lower hybrid frequency using only the electron and ion gyrofrequencies [*Olsen et al.*, 1987]. It only works under the approximation of dense plasma; otherwise it provides only an upper estimate of the lower hybrid frequency.

Figure 3 shows strong diurnal variation in the frequency band above the sixth harmonic of H^+ cyclotron frequency (silver line). The frequencies which show dayside enhancement extend from 150 Hz to 600 Hz. Figure 3b highlights the change in power spectral density with MLT in this range of frequencies with a peak in the morning sector and the lowest values occurring across the nightside. This frequency band includes equatorial noise/plasmaspheric hiss. The diurnal variation in plasmaspheric hiss is attributed to keV electron injection into the outer plasmasphere on the dayside in conjunction with substorms and to whistler mode chorus, which is known to be a source of plasmaspheric hiss, which cannot propagate into the

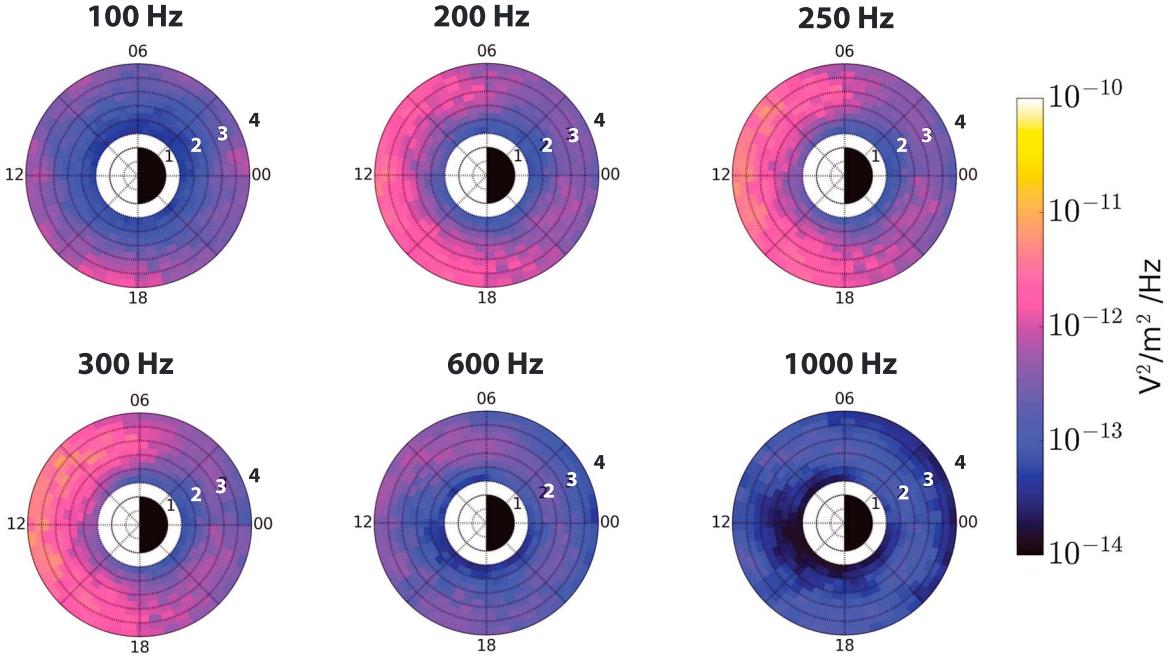

Figure 4. Median equatorial noise electric field power spectral densities at different frequency bands from EMFISIS. Each frequency band was sorted by 0.25 L shell and 0.5 MLT from February 2013 to April of 2015 at times when $Kp < 3$.

plasmasphere on the nightside due to stronger Landau damping caused by higher suprathermal electron flux [*Bortnik et al.*, 2007; *Li et al.*, 2013; *Chen et al.*, 2014; *Li et al.*, 2015]. Diurnal variation is also common in equatorial noise, and proton ring distributions can provide a source of free energy ring velocity (plus/minus a factor of 2 above or below the Alfvenic speed) and generate equatorial noise [*Chen et al.*, 2010, 2011; *Hrbáčková et al.*, 2015].

Figure 4 highlights the power spectral densities for frequencies below 1000 Hz. Using data from February 2013 to April 2015, EMFISIS WFR frequency channels were binned by 0.25 L shell and 0.5 MLT for quiet times when $Kp < 3$. We did not set a limit on the satellite's magnetic latitude in Figure 4. The wave amplitudes peak beyond 150 Hz, with a dayside maximum at all L shells beginning at $f = 200$ Hz and continuing through $f = 300$ Hz. At 1000 Hz, the strong diurnal variation is absent, with a minimum at $L < 3$ dayside MLTs.

3. Quantitative Relationship Between Wave Amplitude and Low-Energy Ions

In this section, we show how the Van Allen Probes observations dovetail with a resonant interaction occurring between low-energy ions and 150–600 Hz waves. Figure 5 compares the median wave power spectral densities at harmonics of the H^+ cyclotron frequency with median H^+ 1–10 eV partial densities at all MLTs for different L shells from February 2013 to April 2015. Figure 5a shows $L = 2.0$, Figure 5b shows $L = 2.5$, and Figure 5c shows $L = 3.0$. For each 4 s measurement of the magnetic field, the gyrofrequency and harmonics of the gyrofrequency were calculated and then the electric field power spectral density at the nearest frequency to the gyrofrequency was extracted and binned.

The partial density and wave power spectral density behave differently at each of the L shells. At $L = 2.0$, The sixth and tenth harmonic wave power spectral density begin to decline at MLT = 14, dropping to approximately 10^{-12} $V^2/m^2/Hz$ between MLT = 19 to MLT = 4. The wave power spectral densities increase in three stages at MLT = 4, 6, and 10 before reaching approximately 10^{-11} $V^2/m^2/Hz$ across the dayside. The sixteenth harmonic wave power spectral density is largely flat with little diurnal variation. The 1–10 eV H^+ density has a maximum at MLT = 6, beginning to increase at approximately MLT = 4. The density gains and losses do not precisely follow the power spectral densities, but both exhibit general diurnal variation.

For $L = 2.5$, the sixth, tenth, and sixteenth harmonic power spectral densities show the most diurnal variation, varying between approximately 10^{-11} $V^2/m^2/Hz$ from MLT = 6 to MLT = 16 and approximately 10^{-12} $V^2/m^2/Hz$ from MLT = 17 to MLT = 3. The different harmonic power spectral densities also follow each other closely with very similar power spectral densities at different MLTs. The partial density also shows the most diurnal variation of the three L shells shown, peaking from MLT = 6 to MLT = 22. The rise of the tenth and sixteenth harmonics of the H^+ gyrofrequency occur before the rise in the partial density, although the peak power spectral density occurs after the partial density has risen above 10^1 cm^{-3}.

Figure 5c shows the least diurnal variation of the sixth, tenth, and sixteenth harmonic power spectral densities. The heightened dayside power spectral densities occur from MLT = 6 to MLT = 14, and the nightside low extends from MLT = 20 to MLT = 3. The sixteenth harmonic is strongest at this L shell, whereas the sixth and tenth harmonic are much lower. The 1–10 eV density takes much longer to reach the high dayside values at this L shell, not reaching peak value until MLT = 9 after a gradual increase starting at MLT = 1.

There are many factors contributing to the partial density increases in Figure 5. It is important to note that harmonic cyclotron resonance occurs at multiple frequencies and heats the ions differently based on the degree of the harmonic and the background magnetic field conditions [*Schmitt*, 1976; *Mauk et al.*, 1981]. So in considering how power spectral densities at different harmonics affect the 1–10 eV H^+ partial densities across MLTs, a holistic approach should be taken. For example, at $L = 2.5$ where all the power spectral densities are high, the cumulative heating impact on the 1–10 eV ions from equatorial noise will be greater than at $L = 3.0$ where the sixteenth harmonic has a higher-power spectral density dayside value than the other harmonics. Also, at L shells closer to Earth, the ionospheric contribution is greater and topside ionospheric plasma is transported into the equatorial plasmasphere faster.

We developed a binary contingency table test to quantify if there was a connection between waves with power spectral density above a certain level and high H^+ fluxes. Figure 6 shows the outcome of our threshold test. Each panel of Figure 6 shows the percentage of each contingency table element based on MLT and L shell location. The grid is divided into 0.25 L shell bins between 1.5 and 4 and 0.5 MLT bins between 0 and 24. The threshold bars were 10^8 cm^{-2} s^{-1} sr^{-1} keV^{-1} for H^+ 2.5 eV fluxes and 10^{-12} $V^2/m^2/Hz$ for EMFISIS power

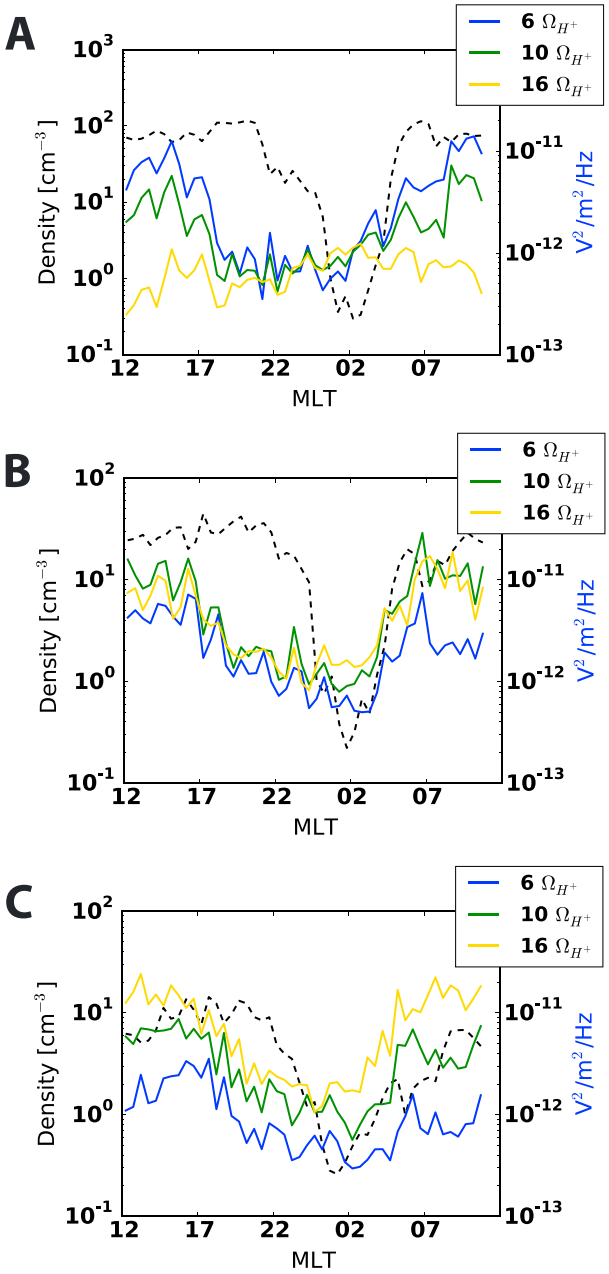

Figure 5. The blue, green, and gold lines are the median electric field power spectral density measured by EMFISIS from February 2013 to April 2015 for the sixth harmonic, tenth harmonic, and sixteenth harmonic of the H^+ gyrofrequency, approximately 100–250 Hz. The different panels show different L shells: (a) $L = 2.0$, (b) $L = 2.5$, and (c) $L = 3.0$. The dashed black line is the median H^+ partial 1–10 eV density over the same time period at the same L shell. Both the power spectral densities and H^+ partial densities were binned by 0.25 L shell and 0.5 MLT.

spectral densities at 250 Hz. The power spectral density boundary is based on the electric field power spectral densities necessary for observable transverse heating of a few eV per hour in the $2 < L < 3$ region [*Singh and Hwang*, 1987]. The flux threshold is based on measured HOPE fluxes at all MLTs for this energy channel.

The High Wave and Particle category denotes HOPE H^+ fluxes of 10^8 cm^{-2} s^{-1} sr^{-1} keV^{-1} or greater and a power spectral density of 10^{-12} V^2/m^2/Hz or greater. The Low Wave and Particle section denotes ion fluxes less than 10^8 cm^{-2} s^{-1} sr^{-1} keV^{-1} and power spectral densities less than 10^{-12} V^2/m^2/Hz. Only High Wave occurs where the power spectral densities are greater than 10^{-12} V^2/m^2/Hz, but the ion fluxes are less than 10^8 cm^{-2} s^{-1} sr^{-1} keV^{-1}. Only High Particle occurs when power spectral densities are less than 10^{-12} V^2/m^2/Hz and the ion fluxes are greater than 10^8 cm^{-2} s^{-1} sr^{-1} keV^{-1}.

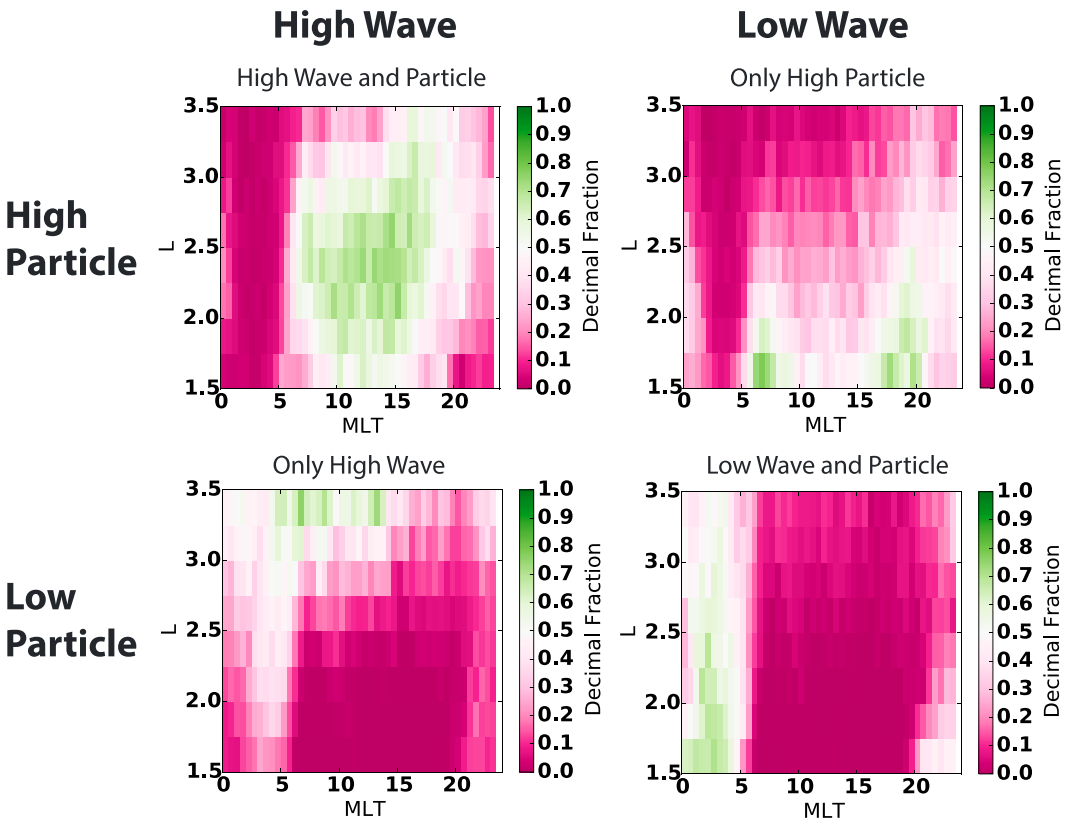

Figure 6. Binary contingency table results of median HOPE 2.5 eV fluxes and EMFISIS electric field power spectral densities at 250 Hz. The study used data from February 2013 to April 2015 which was sorted into 0.25 L shell and 0.5 MLT bins. The High Wave and Particle category denotes HOPE H^+ fluxes of 10^8 cm^{-2} s^{-1} sr^{-1} keV^{-1} or greater and a power spectral density of 10^{-12} $V^2/m^2/Hz$ or greater. The Low Wave and Particle section denotes ion fluxes less than 10^8 cm^{-2} s^{-1} sr^{-1} keV^{-1} and power spectral densities less than 10^{-12} $V^2/m^2/Hz$. Only High Wave occurs where the power spectral densities are greater than 10^{-12} $V^2/m^2/Hz$ but the ion fluxes are less than 10^8 cm^{-2} s^{-1} sr^{-1} keV^{-1}. Only High Particle occurs when power spectral densities are less than 10^{-12} $V^2/m^2/Hz$ and the ion fluxes are greater than 10^8 cm^{-2} s^{-1} sr^{-1} keV^{-1}. The color of each bin reflects the percentage of the bins that lie in each respective category.

There are several key ideas that emerge from Figure 6. When ion fluxes on the dayside are high, in most cases between L shells of 1.5 and 3.25 and MLTs between 5 and 20, the EMFISIS power spectral densities will be high and vice versa. This relationship is demonstrated by the High Wave and Particle contingency outcome, where high percentages (>70%) are seen in these L shell/MLT bins. On the other hand, the Low Wave and Particle category shows us that in the postmidnight region between 0 and 5 MLT and 1.5 to 3.5 L shell, the opposite is seen with approximately equal occurrence frequency; low ion fluxes are accompanied by low-power spectral densities.

The Only High Particle and Only High Wave outcomes of the threshold test reveal the areas subject to extenuating factors. The Only High Wave, where ion fluxes are low despite high-power spectral densities, occurs at higher L shells across many MLTs. We attribute this largely to the declining ion densities from the conservation of the second adiabatic invariant at higher L shells, so the threshold of 10^8 cm^{-2} s^{-1} sr^{-1} keV^{-1} is no longer a fair threshold mark at $L > 3$. The Only High Particle outcome, where power spectral densities are low but the particle fluxes are high, occurs at high percentages for low L shells at MLTs of 5 to 20 and at higher L shells around MLT = 18. We attribute this effect to ionospheric influence. From this binary contingency table, we can see that there is a clear connection between wave amplitudes and high H^+ fluxes.

We supplement this statistical result with a case study to show the relationship between dayside 1–10 eV H^+ flux enhancement and high wave amplitudes. Figure 7 highlights from 9:00 to 11:30 UT on 2 July 2013, when the Van Allen Probes A crossed the postmidnight sector at $2 < L < 3$ on the outbound leg of the orbit. Figure 7a shows the EMFISIS frequency spectrogram for the electric field component of the waves over the same time period between 100 and 800 Hz. Figure 7b is the singular value decomposition (SVD) ellipticity based on the

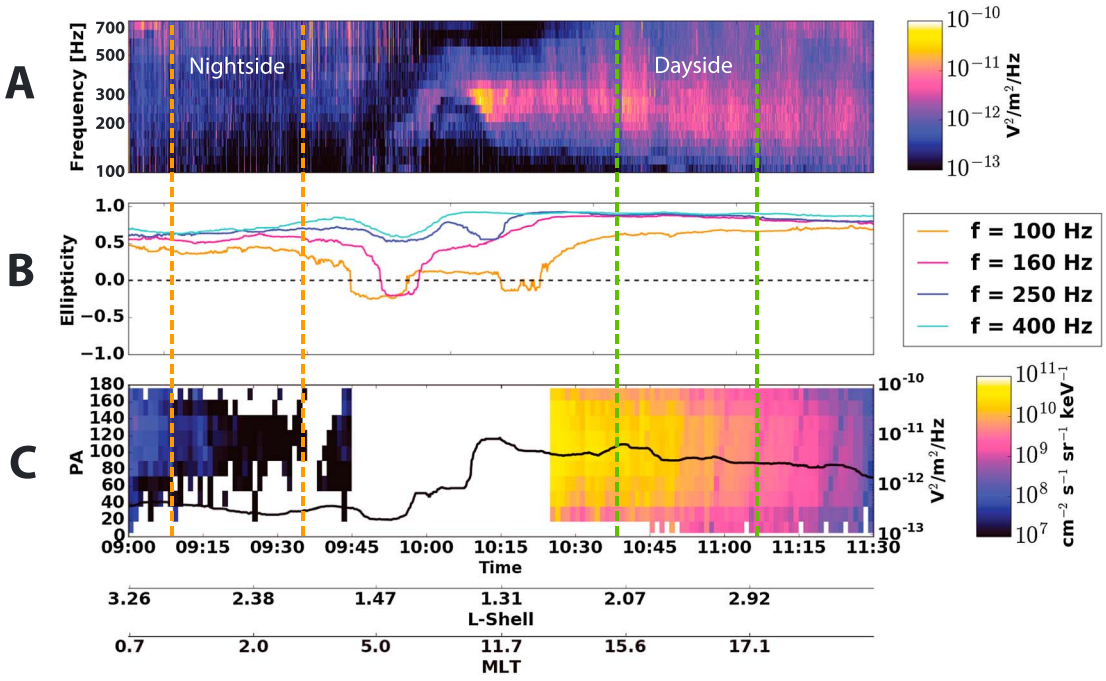

Figure 7. Case study on 2 July 2013 from 9 to 11:30 UT with Van Allen Probes A data. (a) The EMFISIS WFR spectra between 100 and 700 Hz. (b) The ellipticity calculated using singular value decomposition, where +1 indicates right-hand polarized waves, 0 is linearly polarized waves, and −1 is left-hand polarized waves. (c) The H^+ 3.38 eV energy channel differential number fluxes measured in each pitch angle bin over this time interval. The black line is 250 Hz power spectral density. In all panels, the orange dotted lines demarcate where $2 < L < 3$ where $1 < \text{MLT} < 4$ and the green dotted lines highlight where $2 < L < 3$ on the dayside at $15 < \text{MLT} < 18$.

magnetic component of the 250 Hz waves during this time period [*Santolik et al.*, 2003]. The ellipticity indicates the polarization of the wave, with −1 as a left-hand polarized wave, 1 as a right-hand polarized wave, and 0 as a linearly polarized wave. Figure 7c is the pitch angle spectrogram from HOPE for the 3.38 eV energy channel. The black line is the 250 Hz power spectral density. In Figures 7a–7c, the orange dotted lines highlight the postmidnight sector between $2 < L < 3$ and the pink dotted lines highlight the $2 < L < 3$ afternoon ($15 < \text{MLT} < 18$) sector.

From Figures 7a–7c, there is an enhanced population around PA = 90° between 10:25 and 11:30 UT. At this same time, there are enhanced power spectral densities at or near the sixth harmonic of the H^+ cyclotron frequency. The waves in the equatorial noise frequency range, however, are primarily right-hand polarized, indicating plasmaspheric hiss. In the postmidnight sector, there is also an absence of high-power spectral densities and the pitch angle spectrograms reveal a relative minima in the PA = 90° population in this region. The overall fluxes in the 3.38 eV energy range are severely depleted between 9:00 and 9:45 UT compared to the 10:25–11:30 UT 3.38 eV fluxes.

Figure 7c also shows relatively low 250 Hz power spectral densities in the postmidnight sector compared to the inbound orbit power spectral densities and a near-constant refilling population from the 0° and 180° pitch angle fluxes. This case study shows an example of nightside observations of low-power spectral densities paired with little to no PA = 90° H^+ population, as well as dayside observations when both of these values are high. This provides additional evidence supporting the idea that plasma waves could be heating the low-energy ions. This theory is supported by previous results in the literature [*Curtis*, 1985; *Olsen et al.*, 1987; *Singh and Hwang*, 1987; *Horne et al.*, 2000].

4. Polarization Reveals That it is Mostly Plasmaspheric Hiss

However, there is conclusive evidence that these waves between 150 and 600 Hz at $2 < L < 3$ with large power spectral densities are plasmaspheric hiss. Figure 8 shows the median magnetic field ellipticity of 614 days of available data from both Van Allen Probes A and B (double counting, so approximately 307 unique days from each satellite) between February 2013 and April 2015 without distinguishing times of low/high *Kp*.

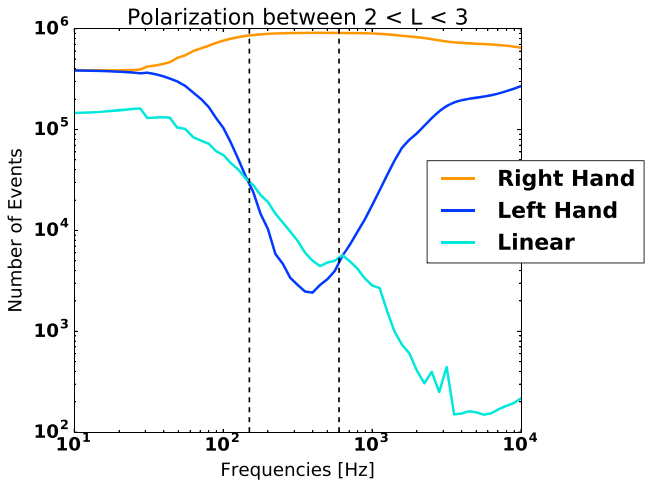

Figure 8. Using 614 days of data from both RBSP-A and RBSP-B (double counting, so approximately 307 unique days), we use ellipticity to determine the sense of the waves in addition to the polarization. Left-hand waves are defined as having ellipticity <−0.2, right-hand waves as having ellipticity >0.2, and linear polarization as waves with ellipticity falling between −0.2 and 0.2. The dotted lines highlight between 150 Hz and 600 Hz, where we see the peak wave amplitudes. Each event is a 1 s measurement at $2 < L < 3$.

Left-hand waves are defined as having ellipticity <−0.2, right-hand waves as having ellipticity >0.2, and linear polarization as waves with ellipticity falling between −0.2 and 0.2 [*Santolík et al.*, 2004; *Li et al.*, 2015]. We only take times where planarity >0.5. The dotted lines highlight between 150 Hz and 600 Hz, where we see the peak wave amplitudes. Each event is a 1 s measurement at $2 < L < 3$. Figure 8 shows that approximately 1% of the wave measurements at $2 < L < 3$ at frequencies of 150 to 600 Hz are linearly polarized or left-hand polarized.

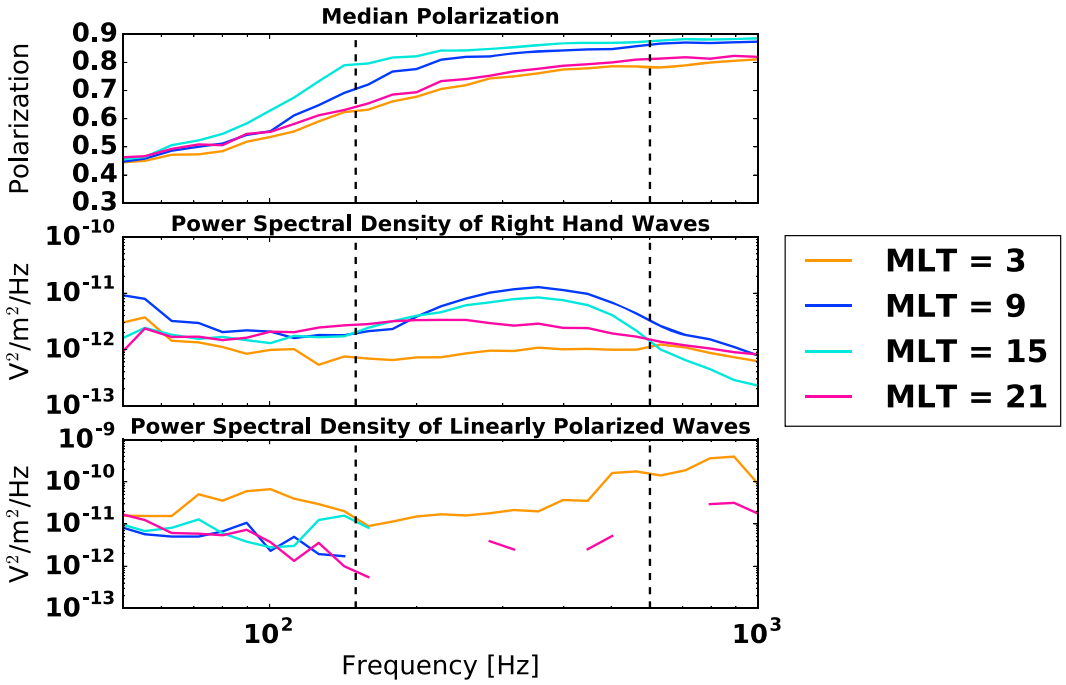

Figure 9. The median polarization and power spectral density of right-hand waves versus linearly polarized waves at $L = 2.5$ at MLT = 3, 9, 15, and 21 from February 2013 to April 2015. (top) The median polarization of all the waves between 0 and 90°. (middle) The power spectral density of waves with polarization greater than 0.7, which here we know from case studies are right-hand polarized waves. (bottom) The linearly polarized waves with polarization <0.2. The dotted lines highlight between 150 Hz and 600 Hz.

Figure 9 shows the median polarization and power spectral density of right-hand waves versus linearly polarized waves at $L = 2.5$ at MLT = 3, 9, 15, and 21 from February 2013 to April 2015 at times where $Kp < 3$. Figure 9 (top) shows the median polarization, or the ellipticity without sense of direction, of all the waves between 0 and 90°. Figure 9 (middle) shows the power spectral density of waves with polarization greater than 0.7, which we know from case studies and Figure 8 are right-hand polarized waves. They could be left-hand polarized waves since our SVD polarization algorithm can only differentiate between circular and linearly polarized without offering information direction like the limited EMFISIS L4 files can. However, Figure 8 confirms that 99% of measurements are right-hand polarized between 150 and 600 Hz, and Figure 9 contains analyzed data from every day between February 2013 and April 2015 and was screened based on the *Kp* index. Figure 9 (bottom) shows the linearly polarized waves with polarization <0.2. The dotted lines highlight between 150 Hz and 600 Hz.

From Figures 8 and 9, we know waves that show high occurrence probability with elevated 1–10 eV population levels are right-hand polarized waves which would not be cyclotron resonant with ions of these energies. Anomalous resonance between the ions and plasmaspheric hiss was considered, as described by *Tsurutani and Lakhina* [1997], *Tsurutani et al.* [1998], and *Kozyra et al.* [1994, 1995]. However, anomalous resonance requires that the phase velocity of the wave is smaller than the particle parallel velocity, which is in contradiction with our extremely low-energy ions with near PA = 90° and reasonable *k* vector magnitudes in the inner magnetosphere of 10^{-3} m^{-1} [*Walker et al.*, 2015]. Therefore, right-hand plasmaspheric hiss, despite evidence in Figure 6 and suggestion in previous work [*Curtis*, 1985; *Olsen et al.*, 1987; *Singh and Hwang*, 1987; *Horne et al.*, 2000], is not responsible for the variation in the suprathermal 1–10 eV ion population. Underlying left-hand or linearly polarized components of plasmaspheric hiss, however, could be responsible for the ion heating, which will be explored in a follow-up study.

5. Conclusions

We have demonstrated that the 1–10 eV H^+ ions measured by the Van Allen Probes exhibit strong diurnal variation in flux measurements with pitch angles near 90°. In particular, this effect is prominent in lower energy particles as seen in Figure 2. Also, when examining pitch angle fluxes against energy, the low-energy fluxes at near PA = 90° rise first and then the higher-energy equatorially mirroring H^+ fluxes increase in Figure 1. With these factors combined, the depletion of ions described in *Sarno-Smith et al.* [2015] is not actually a loss or a transport effect—it is the result of low-energy ion heating across the dayside, likely due to wave-particle interactions.

We then demonstrated a possible cause for the 1–10 eV ion heating across the dayside—higher-order cyclotron resonance. Enhanced levels of polarized plasma waves between the ion cyclotron frequency and lower hybrid frequency at $2 < L < 3$ showed similar statistical rises and falls as the 1–10 eV ions in this same region. The binary contingency tables demonstrated that times where waves had amplitudes above 10^{-11} $V^2/m^2/Hz$ aligned well with times of high low-energy ions fluxes. In more than 70% of cases on the dayside at $2 < L < 3$, high-power spectral density waves occurred with high particle fluxes. In the postmidnight sector, over 70% of the instances had low power spectral densities and low particle fluxes below $L < 3$.

To further solidify this relationship, a case study was presented where high-power spectral densities at 250 Hz occurred when HOPE measured high PA near 90° populations. In the postmidnight sector, this case study showed that the equatorially mirroring population was at a relative minimum while the 0° and 180° pitch angle bins were at a relative maximum. However, this case study also highlights that these high-power spectral density waves on the dayside at $2 < L < 3$ are right-hand polarized plasmaspheric hiss not linearly polarized equatorial noise. Figures 8 and 9 confirm that the 150–600 Hz waves that exhibit similar diurnal variation to the 1–10 eV ion fluxes are right-hand polarized approximately 99% of the time and would not cyclotron resonate with the 1–10 eV ions.

Open questions still remain. Previous studies connected suprathermal ions with the presence of high-power spectral density equatorial noise in the equatorial plane; however, the polarization analysis performed in our study reveals that these waves at $2 < L < 3$ are primarily plasmaspheric hiss. Nevertheless, the binary contingency table in Figure 6 demonstrated a connection between the 1–10 eV H^+ fluxes and plasmaspheric hiss, so there may be a third variable affecting both plasmaspheric hiss presence and 1–10 eV H^+ energization on the inner plasmasphere dayside. The potential heating of He^+ and O^+ has not been examined in regard to a connection with plasmaspheric hiss. Also, the low-energy electrons (<500 eV) have not been examined in

the Van Allen Probes data set yet in regard to wave activity or in relation to fluctuations in the low-energy 1–10 eV population, similar to the findings of *Knudsen et al.* [1998]. Our study concludes that contrary to prior evidence [*Curtis*, 1985; *Olsen et al.*, 1987; *Singh and Hwang*, 1987; *Horne et al.*, 2000], large power spectral density right-hand waves with frequencies between 150 Hz and 600 Hz in the near-Earth equatorial plane do not interact with the 1–10 eV ion population, although they exhibit similar diurnal variation.

Acknowledgments
The Michigan coauthors would like to thank the University of Michigan Rackham Graduate school, NASA, and the NSF for sponsoring this work under grants NWX11AO60G, NWX144AC02G, AGS-1265651, and AGS-1102863. Work at Los Alamos National Laboratory was performed under the auspices of the U.S. Department of Energy, with support from the NASA Van Allen Probes mission under interagency transfer NNG07EK09I and approved for public release as LA-UR-16-25767. The research at the University of Iowa was supported by JHU/APL contract 921647. Data from HOPE and EMFISIS used to generate figures for this project came from the Van Allen Probes data center at https://emfisis.physics.uiowa.edu/data/index and http://rbsp-ect.lanl.gov/. O. Santolik acknowledges support from grants LH14010, LH15304, and from the Praemium Academiae award.

References

Boardsen, S. A., et al. (2016), Survey of the frequency dependent latitudinal distribution of the fast magnetosonic wave mode from Van Allen Probes Electric and Magnetic Field Instrument and Integrated Science waveform receiver plasma wave analysis, *J. Geophys. Res. Space Physics*, *121*, 2902–2921, doi:10.1002/2015JA021844.

Bortnik, J., R. Thorne, and N. Meredith (2007), Modeling the propagation characteristics of chorus using CRRES suprathermal electron fluxes, *J. Geophys. Res.*, *112*, A08204, doi:10.1029/2006JA012237.

Bortnik, J., R. M. Thorne, and N. P. Meredith (2008), The unexpected origin of plasmaspheric hiss from discrete chorus emissions, *Nature*, *452*(7183), 62–66.

Chen, L., R. M. Thorne, V. K. Jordanova, and R. B. Horne (2010), Global simulation of magnetosonic wave instability in the storm time magnetosphere, *J. Geophys. Res.*, *115*, A11222, doi:10.1029/2010JA015707.

Chen, L., R. M. Thorne, V. K. Jordanova, M. F. Thomsen, and R. B. Horne (2011), Magnetosonic wave instability analysis for proton ring distributions observed by the LANL magnetospheric plasma analyzer, *J. Geophys. Res.*, *116*, A03223, doi:10.1029/2010JA016068.

Chen, L., et al. (2014), Generation of unusually low frequency plasmaspheric hiss, *Geophys. Res. Lett.*, *41*, 5702–5709, doi:10.1002/2014GL060628.

Church, S., and R. M. Thorne (1983), On the origin of plasmaspheric hiss: Ray path integrated amplification, *J. Geophys. Res.*, *88*(A10), 7941–7957.

Curtis, S. (1985), Equatorial trapped plasmasphere ion distributions and transverse stochastic acceleration, *J. Geophys. Res.*, *90*(A2), 1765–1770.

Draganov, A., U. Inan, V. Sonwalkar, and T. Bell (1992), Magnetospherically reflected whistlers as a source of plasmaspheric hiss, *Geophys. Res. Lett.*, *19*(3), 233–236.

Funsten, H., et al. (2014), Helium, oxygen, proton, and electron (hope) mass spectrometer for the Radiation Belt Storm Probes mission, in *The Van Allen Probes Mission*, edited by N. Fox and J. L. Burch, pp. 423–484, Springer, New York.

Gary, S. P., K. Liu, D. Winske, and R. E. Denton (2010), Ion Bernstein instability in the terrestrial magnetosphere: Linear dispersion theory, *J. Geophys. Res.*, *115*, A12209, doi:10.1029/2010JA015965.

Green, J. L., S. F. Fung, S. Boardsen, and H. J. Christian (2005), Distribution and origin of plasmaspheric plasma waves, in *Inner Magnetosphere Interactions: New Perspectives From Imaging*, edited by J. Burch, M. Schulz, and H. Spence, pp. 113–126, AGU, Washington, D. C.

Gurnett, D. A. (1976), Plasma wave interactions with energetic ions near the magnetic equator, *J. Geophys. Res.*, *81*(16), 2765–2770.

Horne, R. B., G. V. Wheeler, and H. S. C. Alleyne (2000), Proton and electron heating by radially propagating fast magnetosonic waves, *J. Geophys. Res.*, *105*(A12), 27,597–27,610.

Hrbáčková, Z., O. Santolík, F. Němec, E. Macúšová, and N. Cornilleau-Wehrlin (2015), Systematic analysis of occurrence of equatorial noise emissions using 10 years of data from the Cluster mission, *J. Geophys. Res. Space Physics*, *120*, 1007–1021, doi:10.1002/2014JA020268.

Kletzing, C., et al. (2014), The Electric and Magnetic Field Instrument Suite and Integrated Science (EMFISIS) on RBSP, in *The Van Allen Probes Mission*, edited by N. Fox and J. L. Burch, pp. 127–181, Springer, New York.

Knudsen, D. J., J. H. Clemmons, and J.-E. Wahlund (1998), Correlation between core ion energization, suprathermal electron bursts, and broadband elf plasma waves, *J. Geophys. Res.*, *103*(A3), 4171–4186.

Kozyra, J., C. Rasmussen, R. Miller, and L. Lyons (1994), Interaction of ring current and radiation belt protons with ducted plasmaspheric hiss: 1. Diffusion coefficients and timescales, *J. Geophys. Res.*, *99*(A3), 4069–4084.

Kozyra, J., C. Rasmussen, R. Miller, and E. Villalon (1995), Interaction of ring current and radiation belt protons with ducted plasmaspheric hiss: 2. Time evolution of the distribution function, *J. Geophys. Res.*, *100*(A11), 21,911–21,919.

Kurth, W., S. De Pascuale, J. Faden, C. Kletzing, G. Hospodarsky, S. Thaller, and J. Wygant (2015), Electron densities inferred from plasma wave spectra obtained by the waves instrument on Van Allen Probes, *J. Geophys. Res. Space Physics*, *120*, 904–914, doi:10.1002/2014JA020857.

Laakso, H., H. Junginger, A. Roux, R. Schmidt, and C. D. Villedary (1990), Magnetosonic waves above FC (H^+) at geostationary orbit: GEOS 2 results, *J. Geophys. Res.*, *95*(A7), 10,609–10,621.

Lennartsson, W., and D. L. Reasoner (1978), Low-energy plasma observations at synchronous orbit, *J. Geophys. Res.*, *83*(A5), 2145–2156.

Li, W., Y. Shprits, and R. Thorne (2007), Dynamic evolution of energetic outer zone electrons due to wave-particle interactions during storms, *J. Geophys. Res.*, *112*, A10220, doi:10.1029/2007JA012368.

Li, W., et al. (2013), An unusual enhancement of low-frequency plasmaspheric hiss in the outer plasmasphere associated with substorm-injected electrons, *Geophys. Res. Lett.*, *40*, 3798–3803, doi:10.1002/grl.50787.

Li, W., Q. Ma, R. Thorne, J. Bortnik, C. Kletzing, W. Kurth, G. Hospodarsky, and Y. Nishimura (2015), Statistical properties of plasmaspheric hiss derived from Van Allen Probes data and their effects on radiation belt electron dynamics, *J. Geophys. Res. Space Physics*, *120*, 3393–3405, doi:10.1002/2015JA021048.

Ma, Q., W. Li, R. M. Thorne, and V. Angelopoulos (2013), Global distribution of equatorial magnetosonic waves observed by THEMIS, *Geophys. Res. Lett.*, *40*, 1895–1901, doi:10.1002/grl.50434.

Ma, Q., W. Li, R. M. Thorne, J. Bortnik, C. Kletzing, W. Kurth, and G. Hospodarsky (2016), Electron scattering by magnetosonic waves in the inner magnetosphere, *J. Geophys. Res. Space Physics*, *121*, 274–285, doi:10.1002/2015JA021992.

Mauk, B., C. McIlwain, and m. L. McPherron (1981), Helium cyclotron resonance within the Earth's magnetosphere, *Geophys. Res. Lett.*, *8*(1), 103–106.

Mauk, B., N. J. Fox, S. Kanekal, R. Kessel, D. Sibeck, and A. Ukhorskiy (2014), Science objectives and rationale for the radiation belt storm probes mission, in *The Van Allen Probes Mission*, edited by N. Fox and J. L. Burch, pp. 3–27, Springer, New York.

Meredith, N. P., R. B. Horne, S. A. Glauert, and R. R. Anderson (2007), Slot region electron loss timescales due to plasmaspheric hiss and lightning-generated whistlers, *J. Geophys. Res.*, *112*, A08214, doi:10.1029/2007JA012413.

Meredith, N. P., R. B. Horne, and R. R. Anderson (2008), Survey of magnetosonic waves and proton ring distributions in the Earth's inner magnetosphere, *J. Geophys. Res.*, *113*, A06213, doi:10.1029/2007JA012975.

Meredith, N. P., R. B. Horne, S. A. Glauert, D. N. Baker, S. G. Kanekal, and J. M. Albert (2009), Relativistic electron loss timescales in the slot region, *J. Geophys. Res.*, *114*, A03222, doi:10.1029/2008JA013889.

Němec, F., O. Santolík, K. Gereová, E. Macúšová, H. Laakso, Y. De Conchy, M. Maksimovic, and N. Cornilleau-Wehrlin (2006), Equatorial noise: Statistical study of its localization and the derived number density, *Adv. Space Res.*, *37*(3), 610–616.

Němec, F., O. Santolík, Z. Hrbáčková, and N. Cornilleau-Wehrlin (2015), Intensities and spatiotemporal variability of equatorial noise emissions observed by the Cluster spacecraft, *J. Geophys. Res. Space Physics*, *120*, 1620–1632, doi:10.1002/2014JA020814.

Olsen, R., S. Shawhan, D. Gallagher, J. Green, C. Chappell, and R. Anderson (1987), Plasma observations at the Earth's magnetic equator, *J. Geophys. Res.*, *92*(A3), 2385–2407.

Perraut, S. (1982), Wave-particle interactions in the ULF range: GEOS-1 and-2 results, *Planet. Space Sci.*, *30*(12), 1219–1227.

Perraut, S., A. Roux, P. Robert, R. Gendrin, J.-A. Sauvaud, J.-M. Bosqued, G. Kremser, and A. Korth (1982), A systematic study of ULF waves above FH+ from GEOS 1 and 2 measurements and their relationships with proton ring distributions, *J. Geophys. Res.*, *87*(A8), 6219–6236.

Quinn, J., and R. Johnson (1982), Composition measurements of warm equatorially trapped ions near geosynchronous orbit, *Geophys. Res. Lett.*, *9*(7), 777–780.

Roux, A., S. Perraut, J. Rauch, C. Villedary, G. Kremser, A. Korth, and D. Young (1982), Wave-particle interactions near ωHe+ observed on board GEOS 1 and 2: 2. Generation of ion cyclotron waves and heating of He+ ions, *J. Geophys. Res.*, *87*(A10), 8174–8190.

Russell, C. T., R. E. Holzer, and E. J. Smith (1970), OGO 3 observations of ELF noise in the magnetosphere: 2. The nature of the equatorial noise, *J. Geophys. Res.*, *75*(4), 755–768.

Santolik, O., M. Parrot, L. Storey, J. Pickett, and D. Gurnett (2001), Propagation analysis of plasmaspheric hiss using Polar PWI measurements, *Geophys. Res. Lett.*, *28*(6), 1127–1130.

Santolík, O., J. Pickett, D. Gurnett, M. Maksimovic, and N. Cornilleau-Wehrlin (2002), Spatiotemporal variability and propagation of equatorial noise observed by Cluster, *J. Geophys. Res.*, *107*(A12), 1495, doi:10.1029/2001JA009159.

Santolik, O., M. Parrot, and F. Lefeuvre (2003), Singular value decomposition methods for wave propagation analysis, *Radio Sci.*, *38*(1), 1010, doi:10.1029/2000RS002523.

Santolík, O., F. Nemec, K. Gereová, E. Macúšová, Y. De Conchy, and N. Cornilleau-Wehrlin (2004), Systematic analysis of equatorial noise below the lower hybrid frequency, *Ann. Geophys.*, *22*, 2587–2595.

Sarno-Smith, L. K., M. W. Liemohn, R. M. Katus, R. M. Skoug, B. A. Larsen, M. F. Thomsen, J. R. Wygant, and M. B. Moldwin (2015), Postmidnight depletion of the high-energy tail of the quiet plasmasphere, *J. Geophys. Res. Space Physics*, *120*, 1646–1660, doi:10.1002/2014JA020682.

Sarno-Smith, L. K., M. W. Liemohn, R. M. Skoug, B. A. Larsen, M. B. Moldwin, R. M. Katus, and J. R. Wygant (2016a), Local time variations of high-energy plasmaspheric ion pitch angle distributions, *J. Geophys. Res. Space Physics*, *121*, 6234–6244, doi:10.1002/2015JA022301.

Sarno-Smith, L. K., B. A. Larsen, R. M. Skoug, M. W. Liemohn, A. Breneman, J. R. Wygant, and M. F. Thomsen (2016b), Spacecraft surface charging within geosynchronous orbit observed by the Van Allen Probes, *Space Weather*, *14*, 151–164, doi:10.1002/2015SW001345.

Schmitt, J. (1976), Nonlinear theory of RF heating at cyclotron harmonics, *Phys. Fluids*, *19*(2), 245–255.

Singh, N., and K. Hwang (1987), Perpendicular ion heating effects on the refilling of the outer plasmasphere, *J. Geophys. Res.*, *92*(A12), 13,513–13,521.

Solomon, J., N. Cornilleau-Wehrlin, A. Korth, and G. Kremser (1988), An experimental study of ELF/VLF hiss generation in the Earth's magnetosphere, *J. Geophys. Res.*, *93*(A3), 1839–1847.

Summers, D., B. Ni, and N. P. Meredith (2007), Timescales for radiation belt electron acceleration and loss due to resonant wave-particle interactions: 2. Evaluation for VLF chorus, ELF hiss, and electromagnetic ion cyclotron waves, *J. Geophys. Res.*, *112*, A04207, doi:10.1029/2006JA011993.

Thorne, R. M., and J. N. Barfield (1976), Further observational evidence regarding the origin of plasmaspheric hiss, *Geophys. Res. Lett.*, *3*(1), 29–32.

Thorne, R. M., E. J. Smith, R. K. Burton, and R. E. Holzer (1973), Plasmaspheric hiss, *J. Geophys. Res.*, *78*(10), 1581–1596.

Tsurutani, B., J. Arballo, G. Lakhina, C. Ho, B. Buti, J. Pickett, and D. Gurnett (1998), Plasma waves in the dayside polar cap boundary layer: Bipolar and monopolar electric pulses and whistler mode waves, *Geophys. Res. Lett.*, *25*(22), 4117–4120.

Tsurutani, B. T., and G. S. Lakhina (1997), Some basic concepts of wave-particle interactions in collisionless plasmas, *Rev. Geophys.*, *35*(4), 491–501.

Tsurutani, B. T., E. J. Smith, and R. M. Thorne (1975), Electromagnetic hiss and relativistic electron losses in the inner zone, *J. Geophys. Res.*, *80*(4), 600–607.

Walker, S., M. Balikhin, D. Shklyar, K. Yearby, P. Canu, C. Carr, and I. Dandouras (2015), Experimental determination of the dispersion relation of magnetosonic waves, *J. Geophys. Res. Space Physics*, *120*, 9632–9650, doi:10.1002/2015JA021746.

Wygant, J., et al. (2013), The electric field and waves instruments on the radiation belt storm probes mission, *Space Sci. Rev.*, *179*(1–4), 183–220.

Young, D., S. Perraut, A. Roux, C. Villedary, R. Gendrin, A. Korth, G. Kremser, and D. Jones (1981), Wave-particle interactions near ωhe+ observed on GEOS 1 and 2 1. Propagation of ion cyclotron waves in He+-rich plasma, *J. Geophys. Res.*, *86*(A8), 6755–6772.